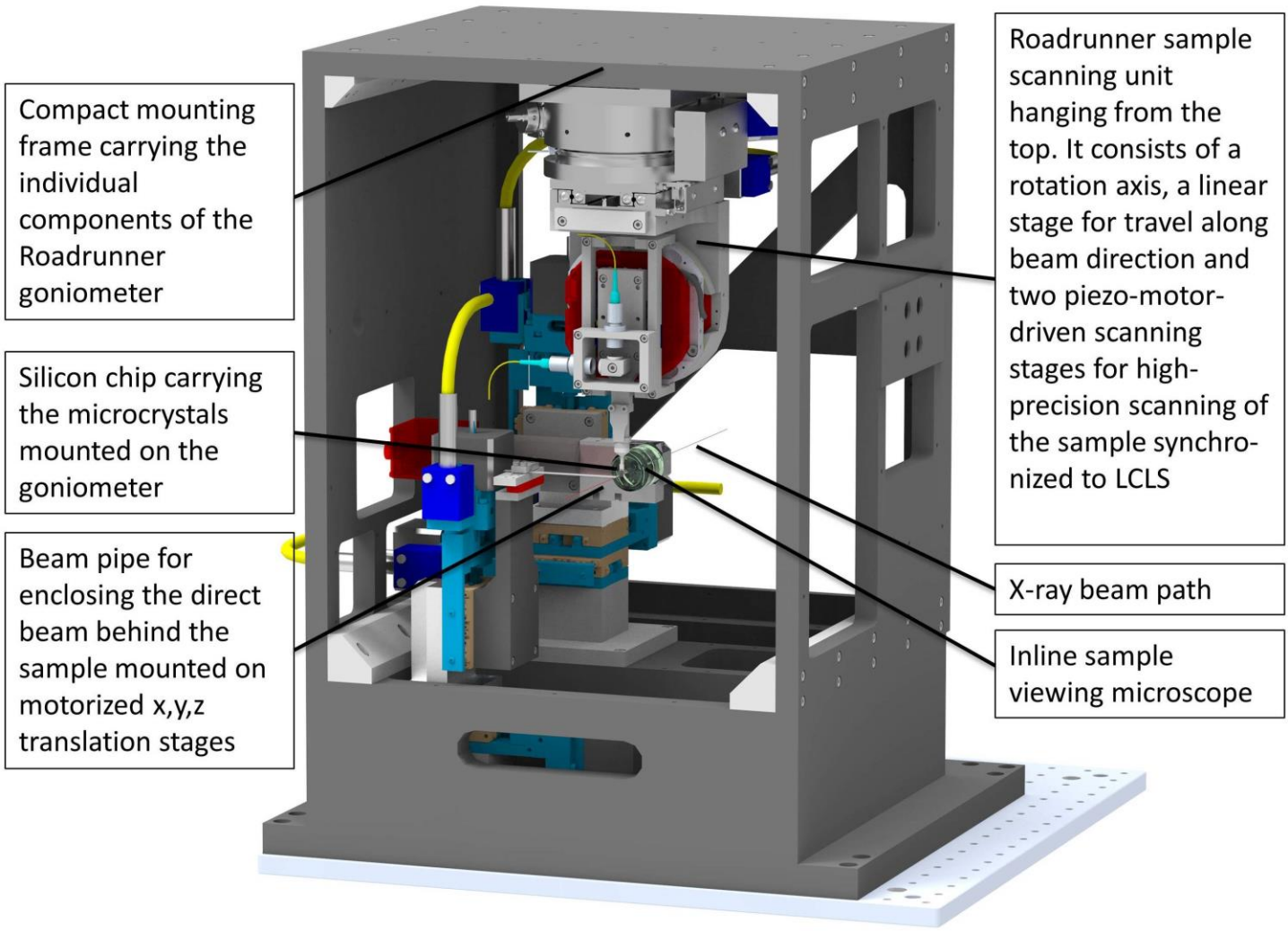


**Supplementary Figure 1**

Technical overview drawing of the Roadrunner goniometer.

The goniometer consists of three main components: an inline sample-viewing microscope, a high-precision scanning unit for fast scanning, and a motorized beam pipe unit. All components are mounted on a common support frame to achieve high mechanical stability. The overall dimensions of the support frame are 350 mm along the beam direction, the height is 515 mm, and the width is 400 mm. The beam and sample height is 250 mm above the base plate. The minimum possible distance between sample and detector surface is 50 mm allowing for the collection of high-resolution diffraction data. For better visibility, the open flow cryostat for measurements at cryogenic temperatures and the nozzle releasing a humidified gas stream for room-temperature measurements are not shown.

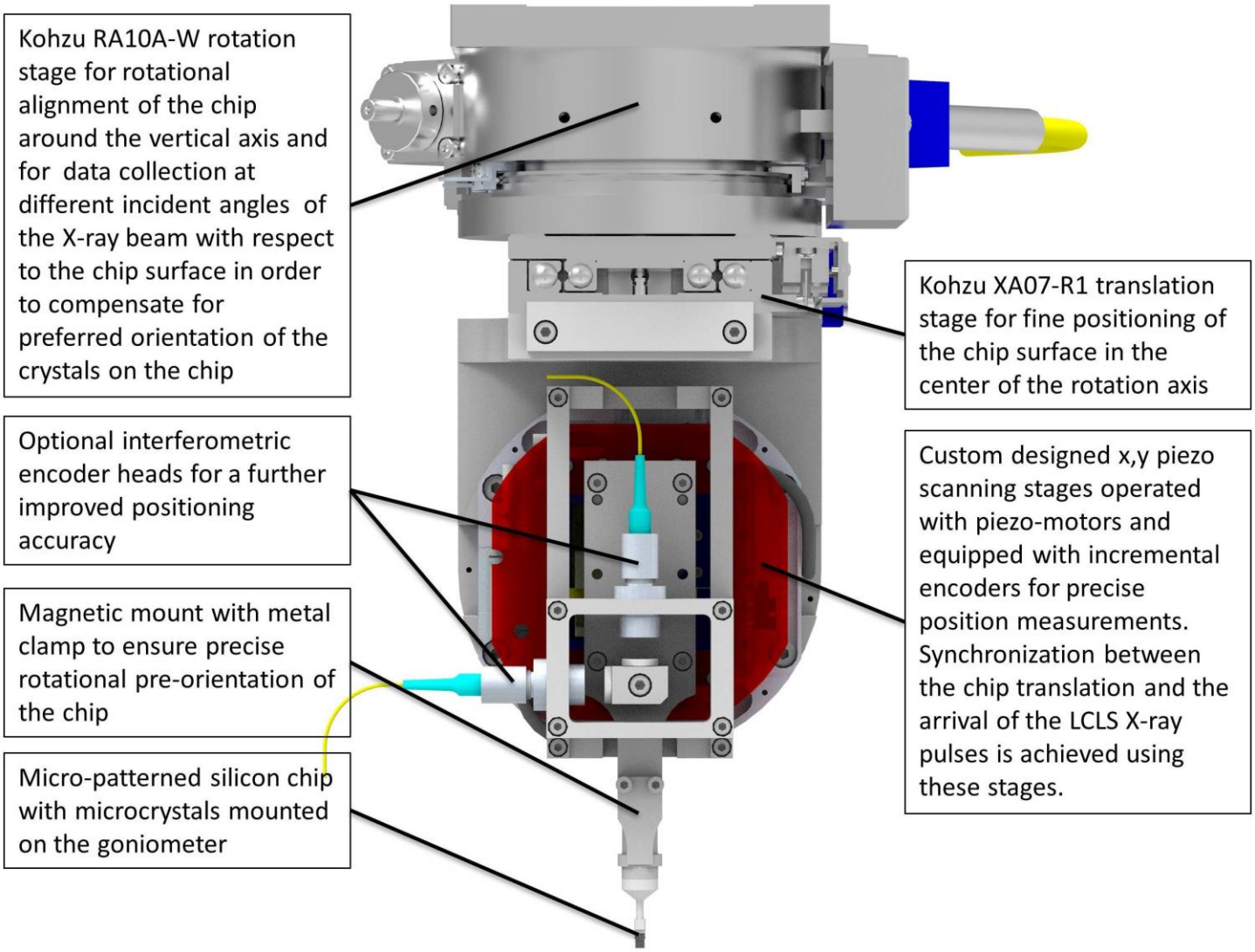


**Supplementary Figure 2**

Technical drawing of the scanning unit of the Roadrunner goniometer.

As illustrated in Supplementary Figure 1, the scanning unit is mounted vertically and hanging from the outer support frame. Upper element of the scanning unit is a Kohzu RA10A-W rotation stage. The rotation axis allows a +/- 60° rotation of the whole scanning unit along the vertical axis. The stage is used for rotational alignment of the chip along the vertical axis and can be further used for rotation of the chip to avoid obtaining incomplete diffraction datasets due to preferred orientation of the crystals on the chip. A stepper motor driven Kohzu XA07-RA translation stage is mounted below the rotation axis, which allows adjustment of the chip along a horizontal axis. This axis is used to position the chip surface in the center of rotation of the vertical rotation axis. The main high-precision scanning unit is mounted below the horizontal translation stage. It consists of two piezo-motor driven translation stages, which are equipped with incremental encoders and allow a fast translation of the chip with a speed of up to 2.5 mm/s. The achievable resolution of the setup is 100 nm. In case even higher resolution is required the scanning stages can be additionally equipped with interferometric sensors. For fast chip scanning synchronized to the arrival of the LCLS pulses only the horizontal axis is used, as this movement is not affected by gravity. The vertical axis is only used for small corrections e.g. arising from a not exact horizontal orientation of the hole pattern. The chip is mounted onto the scanning unit using a magnetic mount. A clamp attached to the magnetic mount is used to ensure the pre-orientation of the chips by allowing mounting of the chip in one angular position only.

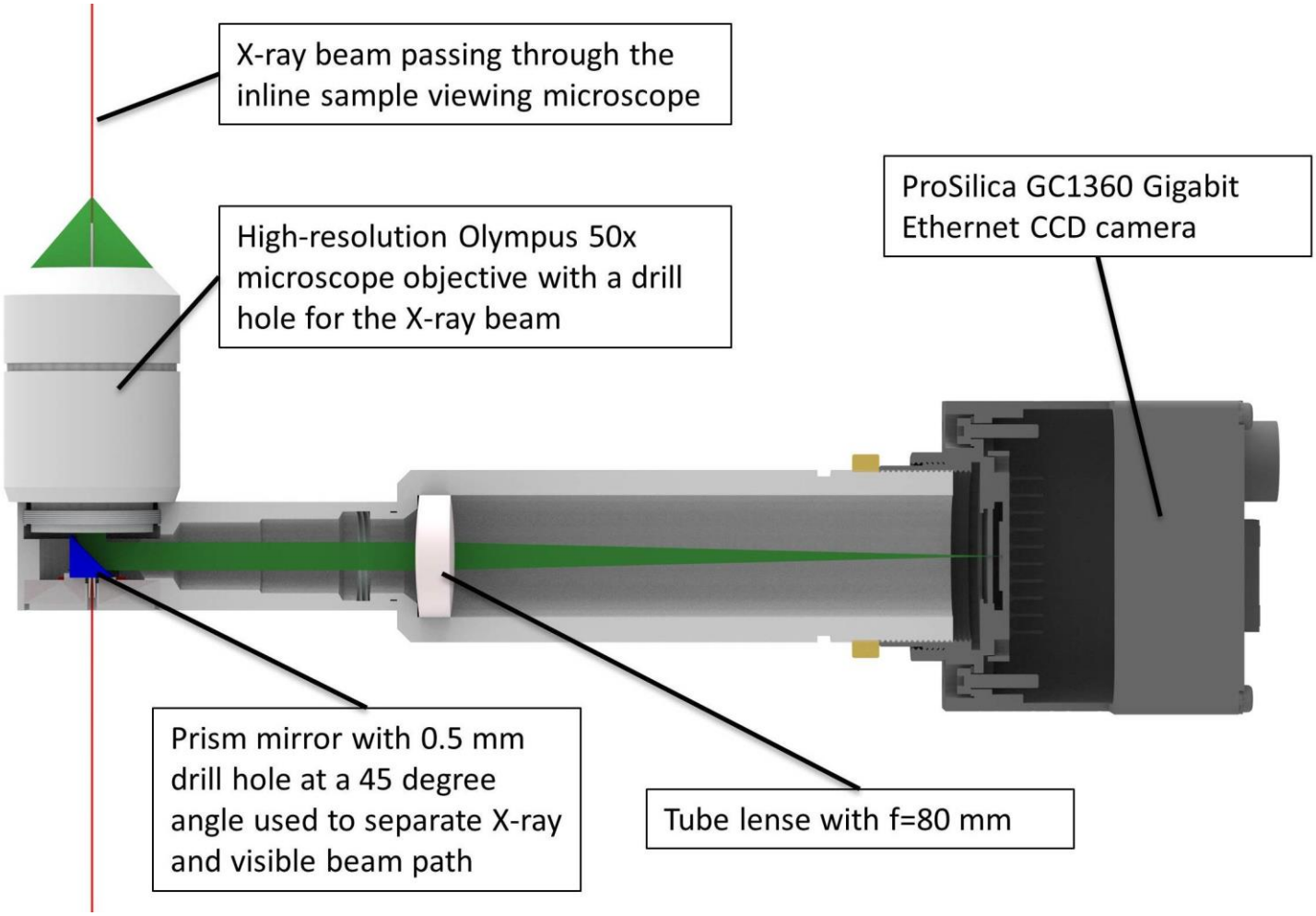


**Supplementary Figure 3**

Technical drawing of the very compact Roadrunner inline sample-viewing microscope.

Main component is an Olympus LMPLFLN50X light microscope objective with 50x magnification and a numerical aperture of NA=0.5 with a 0.5 mm diameter hole through its center for the X-rays to pass through. The X-ray beam path is indicated in red. To reduce scattering background a 0.5 mm outer diameter and 0.35 mm inner diameter molybdenum tube is inserted into the drill hole extending to about 3 mm before the sample position. The optical light path is indicated in green. After leaving the microscope the light path is deflected by 90 degrees using a prism mirror, which is also equipped with a drill hole to pass the X-rays. After exiting the tube lens (f=80 mm), the magnified image of the sample is recorded using a ProSilica GC1360 Gigabit Ethernet CCD camera. The spatial resolution of the microscope setup is better than 1 µm.

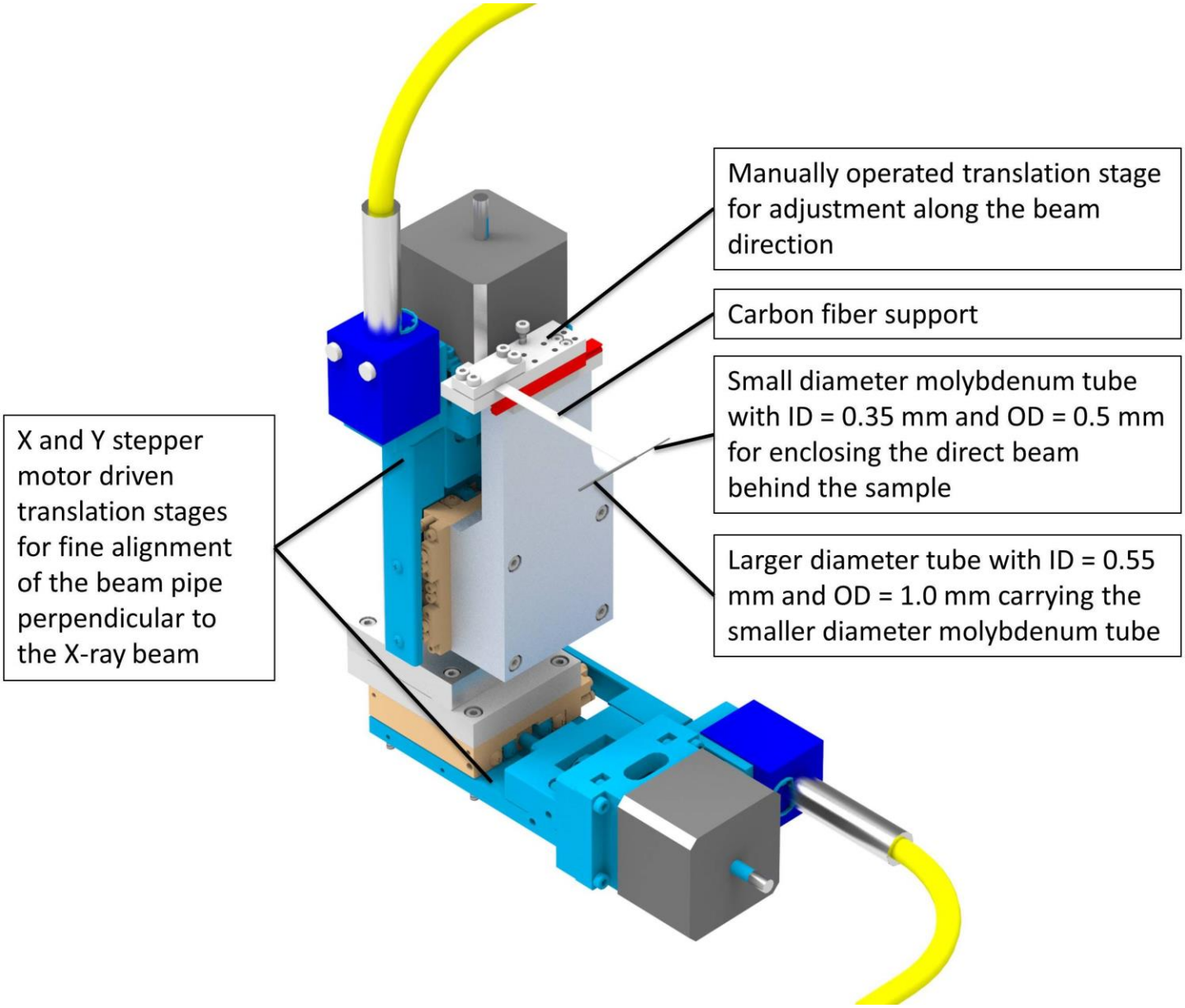


**Supplementary Figure 4**

Technical drawing of the postsample beam pipe unit of the Roadrunner goniometer.

The beam pipe consists of a molybdenum tube with an inner diameter (ID) of 0.35 mm and an outer diameter (OD) of 0.5 mm. The upstream end of the pipe is placed about 15 mm behind the sample. The far end of the smaller diameter tube is inserted into a second larger tube with an ID of 0.55 mm and an OD of 1 mm, which extends several tens of millimeters downstream into the central hole of the CSPAD detector. The larger tube is manually pre-aligned in the direction of the direct beam path. It is mounted on a manually operated translation stage for adjustment along the beam direction. Two stepper motor operated translation stages allow fine adjustment of the beam pipe perpendicular to the X-ray beam and to guarantee that the primary beam is well enclosed by the beam pipe. By enclosing the direct beam shortly behind the sample in the molybdenum tube all X-rays scattered by air on the way down to the detector are absorbed in the beam pipe walls and therefore do not contribute to background scattering onto the detector. This results in a significant reduction of the background level from air scattering.

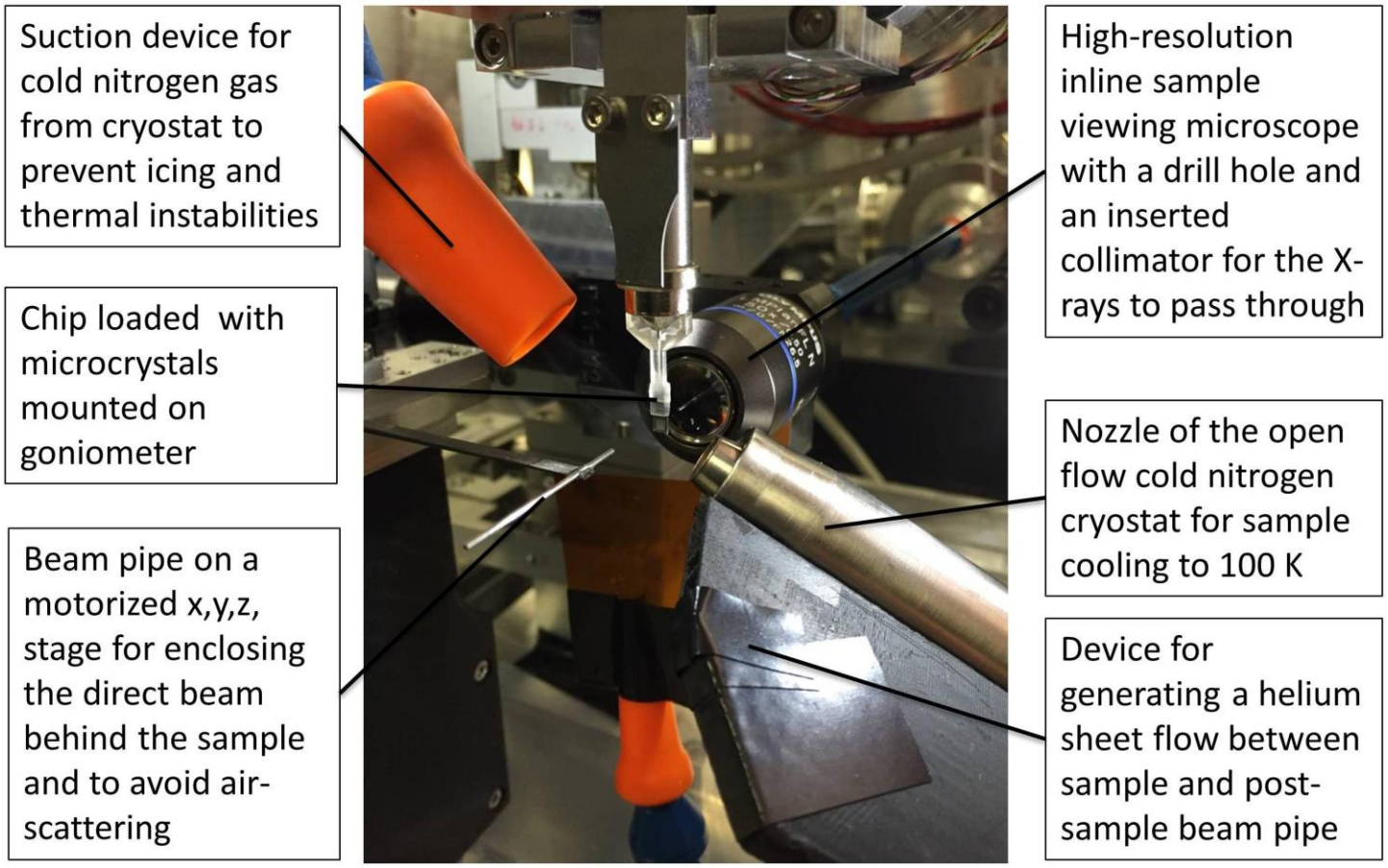


**Supplementary Figure 5**

Picture of the Roadrunner goniometer installed at the XPP instrument at LCLS for measurements at cryogenic temperatures.

The beam first passes through a drill hole in the inline sample viewing microscope used to visualize and align the sample. A molybdenum collimator tube inserted into the drill hole in the objective lens absorbs radiation caused by air scattering in order to reduce background scattering. The silicon chip sample holder is mounted from the top on the high-precision goniometer stage (not shown). The sample is cooled to temperatures down to 80 K by a cold nitrogen gas flow. Behind the sample the direct beam enters a molybdenum beam pipe absorbing X-rays scattered by air. Background scattering is further reduced by generating a helium gas sheet along the primary beam path between the sample and the beam pipe enclosing the direct beam behind the sample. For room-temperature measurements the cold nitrogen gas flow is replaced by a stream of humidified gas to prevent dehydration of the crystals (not shown here).

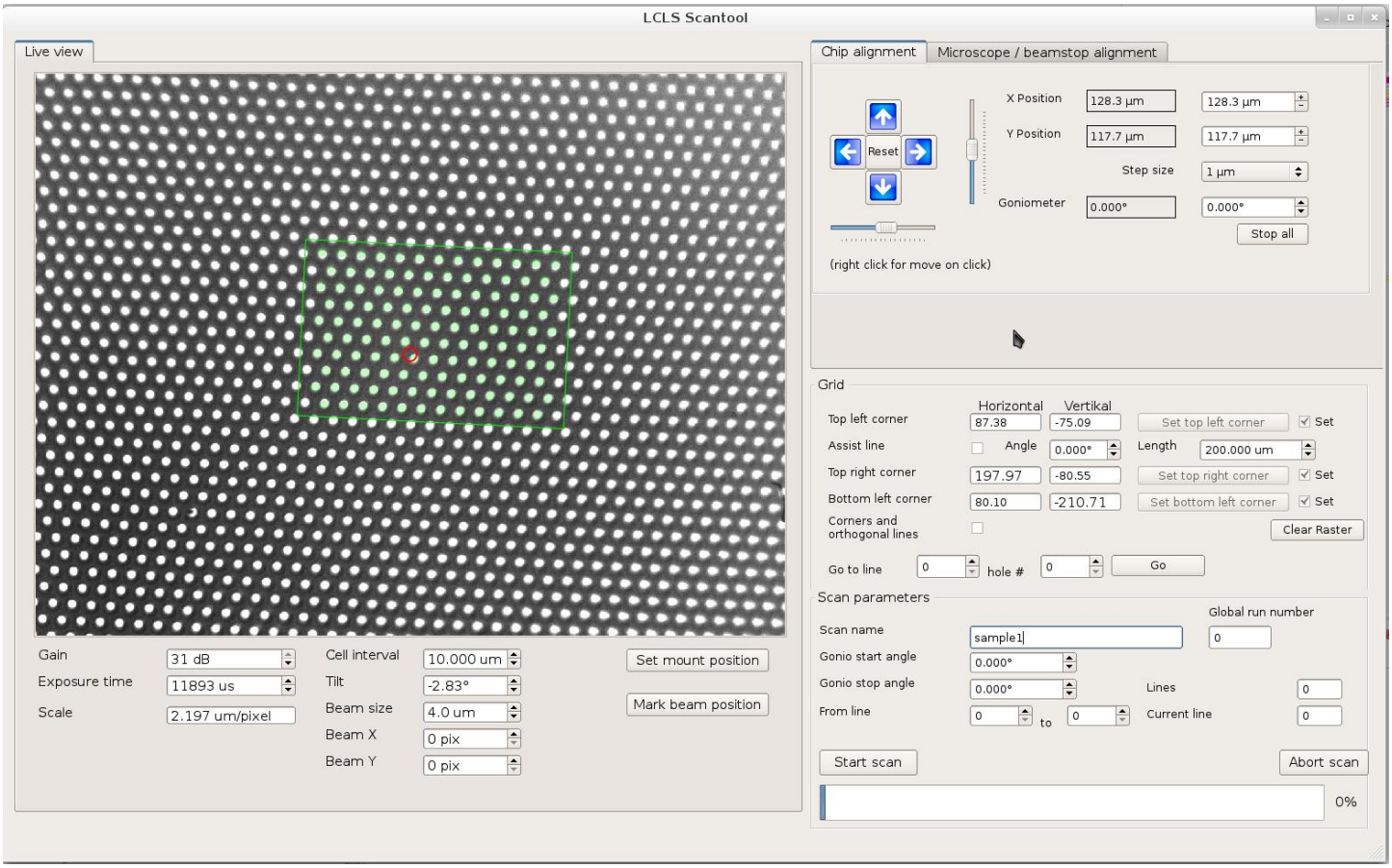


**Supplementary Figure 6**

Graphical user interface of the Roadrunner goniometer.

On the left side of the graphical user interface the image of the inline sample-viewing microscope is displayed – showing a chip mounted on the goniometer. The distance between the pores of the chip shown is 10 µm and the pore diameter ~5 µm. The red dot in the center of the image represents the X-ray beam position. The green and yellow lines are support lines to define the scan grid. Below the microscope image and on the right side of the GUI several control parameters and motor positions are displayed and can be adjusted.

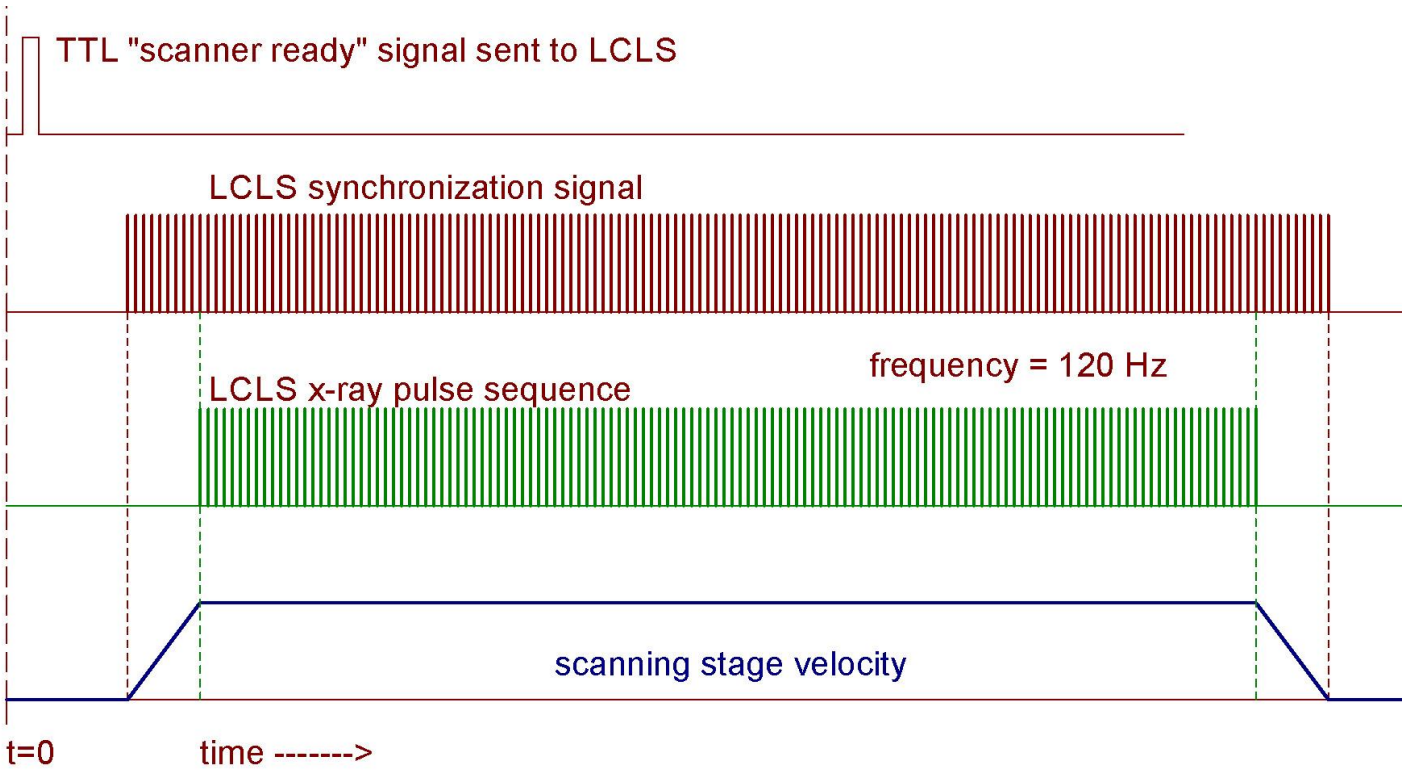


**Supplementary Figure 7**

Synchronization scheme of the fast scanning axis with the timing signal of LCLS.

Once the goniometer is in the right position to perform a line scan a TTL “scanner ready” signal is sent from the goniometer controller to the LCLS control system. When the signal is received by the LCLS control systems it starts sending a predefined sequence of TTL signals co-incident to the X-ray pulse arrival times with a frequency of 120 Hz. At the beginning the pulse picker at XPP is blocking the beam and no X-ray pulses are delivered to the sample. These first timing pulses are used for acceleration of the sample scanner and to synchronize the position of the pores with the beam position and arrival time of the X-ray pulses. Once the pore position is in phase with the arrival of the X-ray pulses the pulse picker opens and X-rays are hitting the crystals located in the pores of the chip and diffraction images are recorded. Once the end of a line is reached, the pulse picker closes and the X-rays are blocked. A few more timing signals are sent out for deceleration of the chip. After no signals are received by the goniometer controller anymore, the goniometer moves to the starting position of the next scan line, sends out the “scanner ready” signal to the controller, which then continues scanning the line in reverse direction and so on. After the number of predefined lines are scanned in a meander-like fashion no “scanner ready’ signal is sent out anymore and data collection is finished.

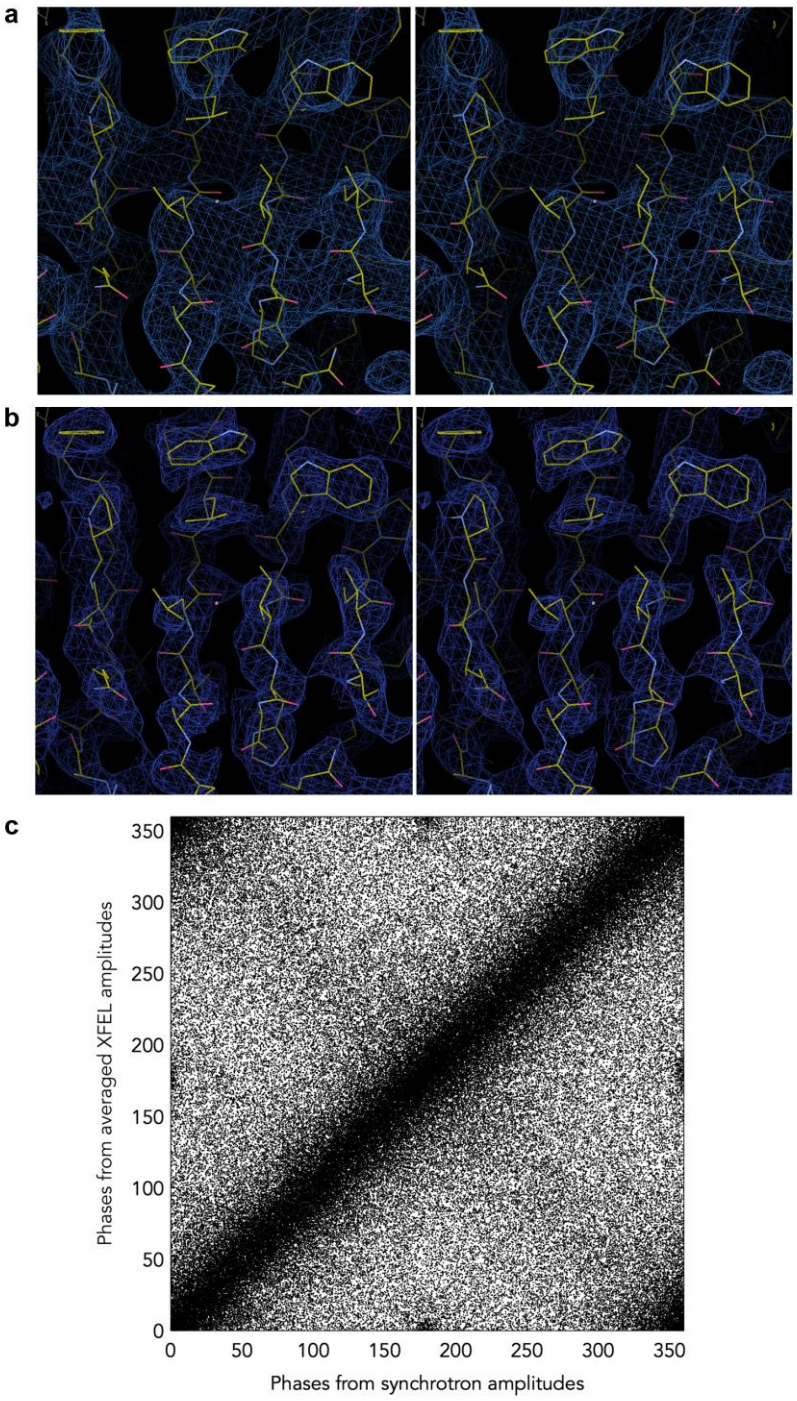


**Supplementary Figure 8**

BEV2 phase extension of XFEL data.

(a) Stereo diagram of a 5-fold real space averaged electron density map at 5 Å resolution prior to phase extension. (b) Electron density map after phase extension to 2.5 Å by cyclic real space averaging and solvent flattening. (c) Scatter plot of phases derived from XFEL data via phase extension and those derived from an averaged map calculated from synchrotron data. Phases are only shown for reflections in the resolution range 5 Å to 2.5 Å.

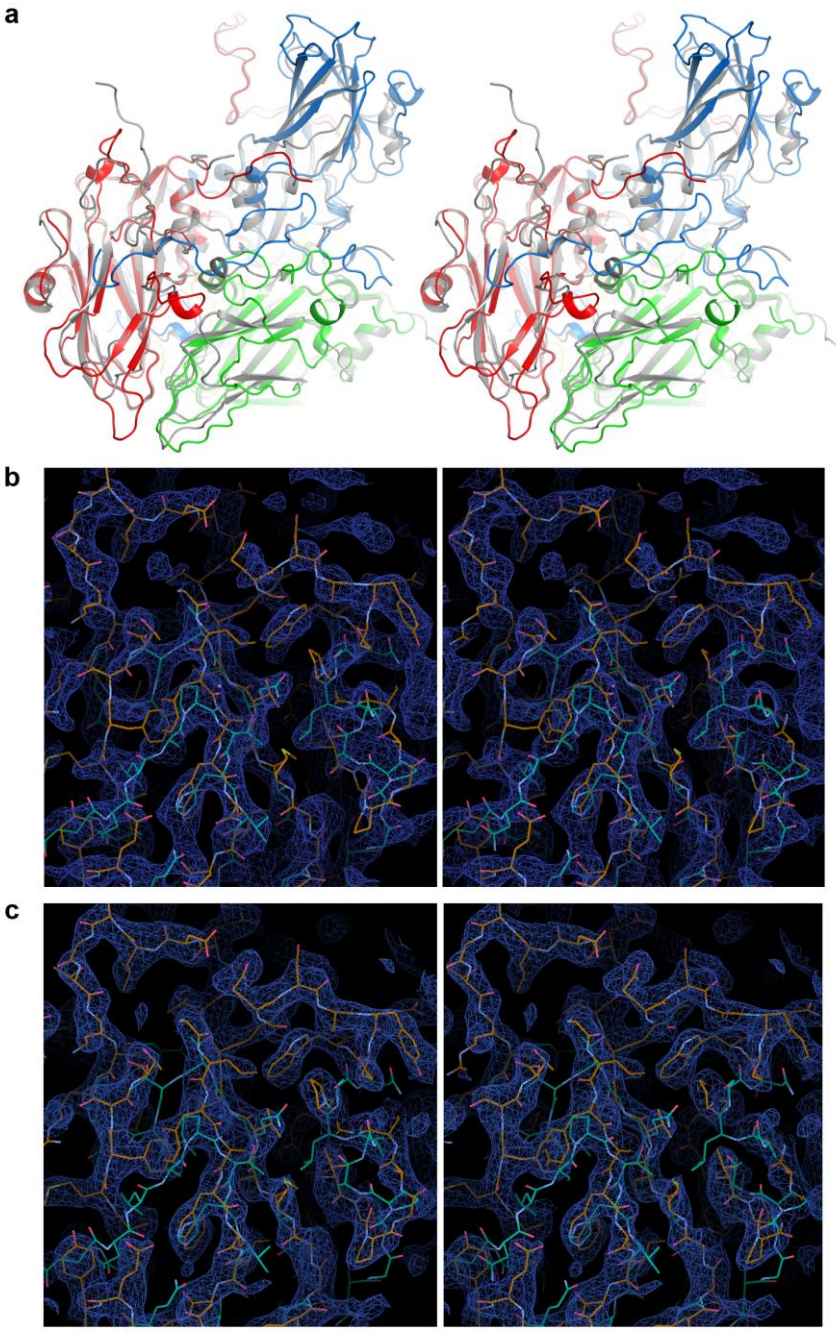


**Supplementary Figure 9**

BEV2 structure determination on the basis of XFEL data by molecular replacement using FMDV A22 as a starting model.

(a) Stereo diagram showing the structural differences between BEV2 and FMDV A22 protomers. VP1, VP2, VP3 and VP4 of BEV2 are shown in blue, green, red and yellow respectively, FMDV A22 in grey. (b & c) Stereo diagram showing the electron density maps for the north wall of the canyon which surrounds the icosahedral 5-fold axes (note that FMDVs do not have such a canyon); (b) shows 5-fold real space averaged maps, (c) shows the map after cyclic real space averaging and solvent flattening. The initial map was calculated using phases derived from the FMDV A22 model at 2.3 Å resolution. The final refined structure of BEV2 is in orange and FMDV A22 in cyan.

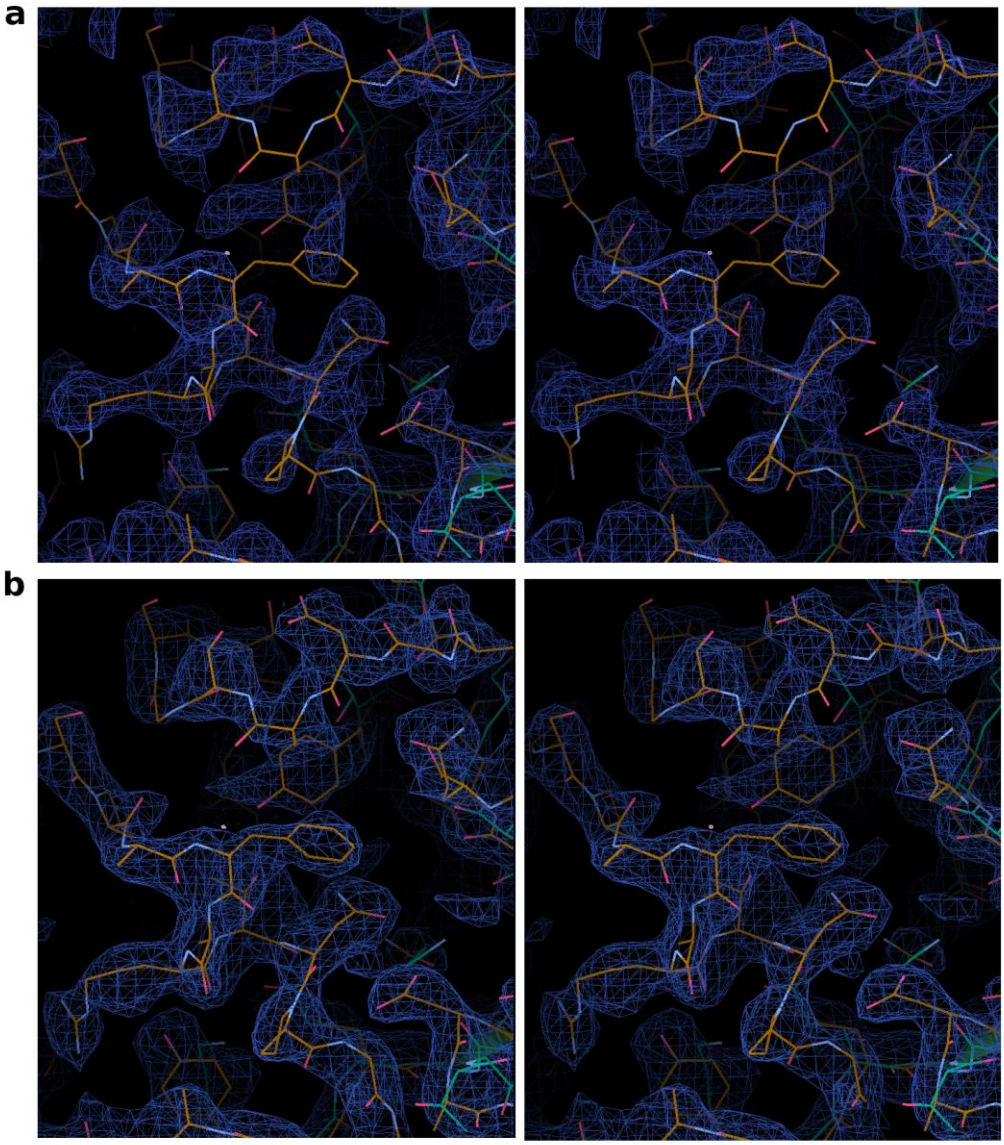


**Supplementary Figure 10**

BEV2 phase refinement.

Stereo images of the electron density map around the south wall of the canyon before (a) and after (b) phase refinement by cyclic averaging. As in Supplementary Figure 9, the shown structure of BEV2 (orange) was obtained by molecular replacement using FMDV A22 as a starting model (cyan). Note the complete elimination of bias.

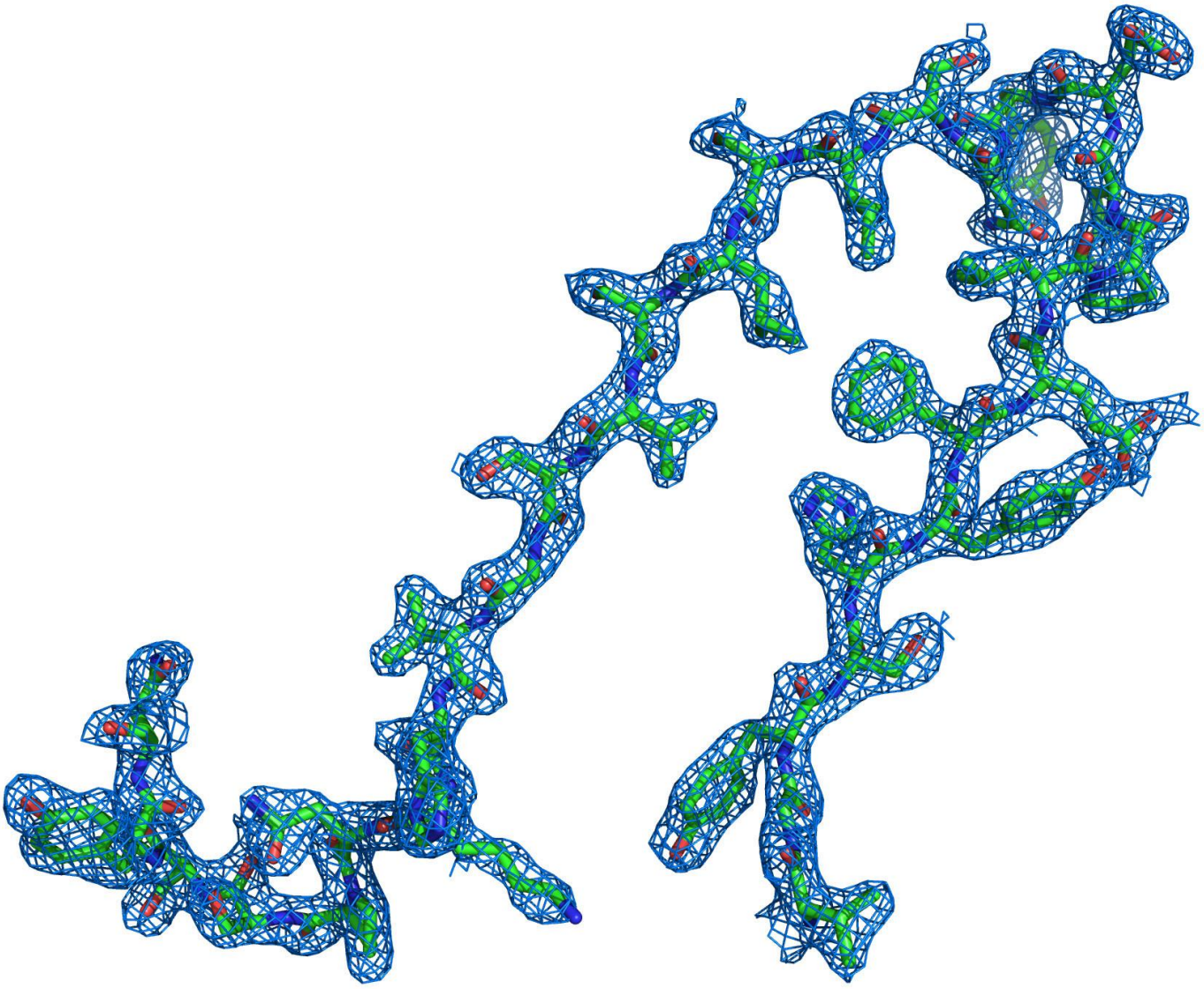

**Supplementary Figure 11**

Refined electron density map for CPV18.

Part of the electron density map ($2F_o$-$F_c$, contoured at 1σ) refined from CPV18 diffraction data, obtained by the presented method of fixed-target serial femtosecond X-ray crystallography. Image is showing residues 160 through 190.

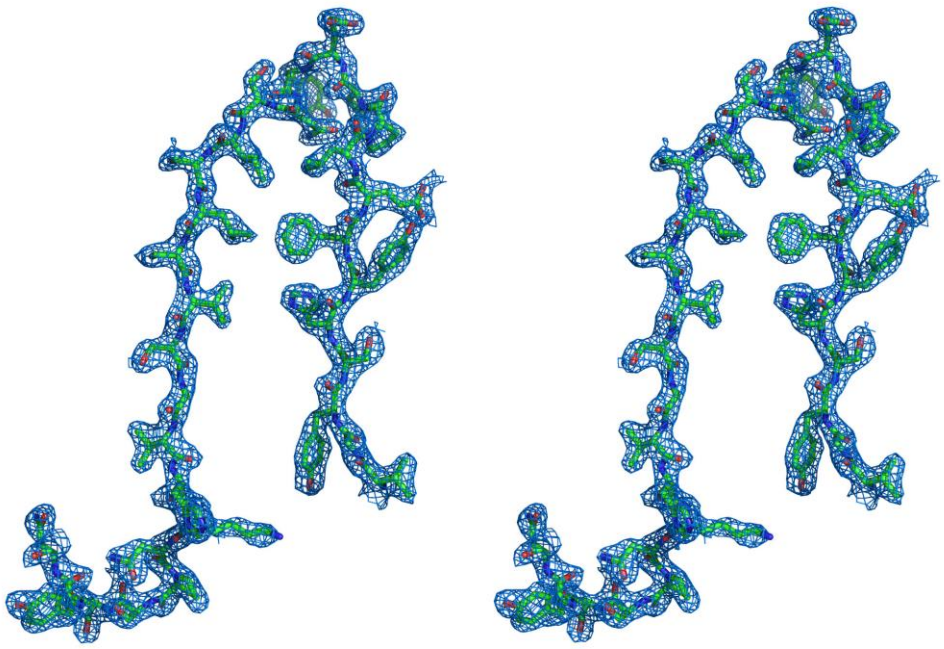

**Supplementary Figure 12**

Stereo view of CPV18 electron density map.

Wall-eyed stereo image of the electron density map of the CPV18 data as shown in Supplementary Figure 11 (2Fo-Fc, contoured at 1σ).

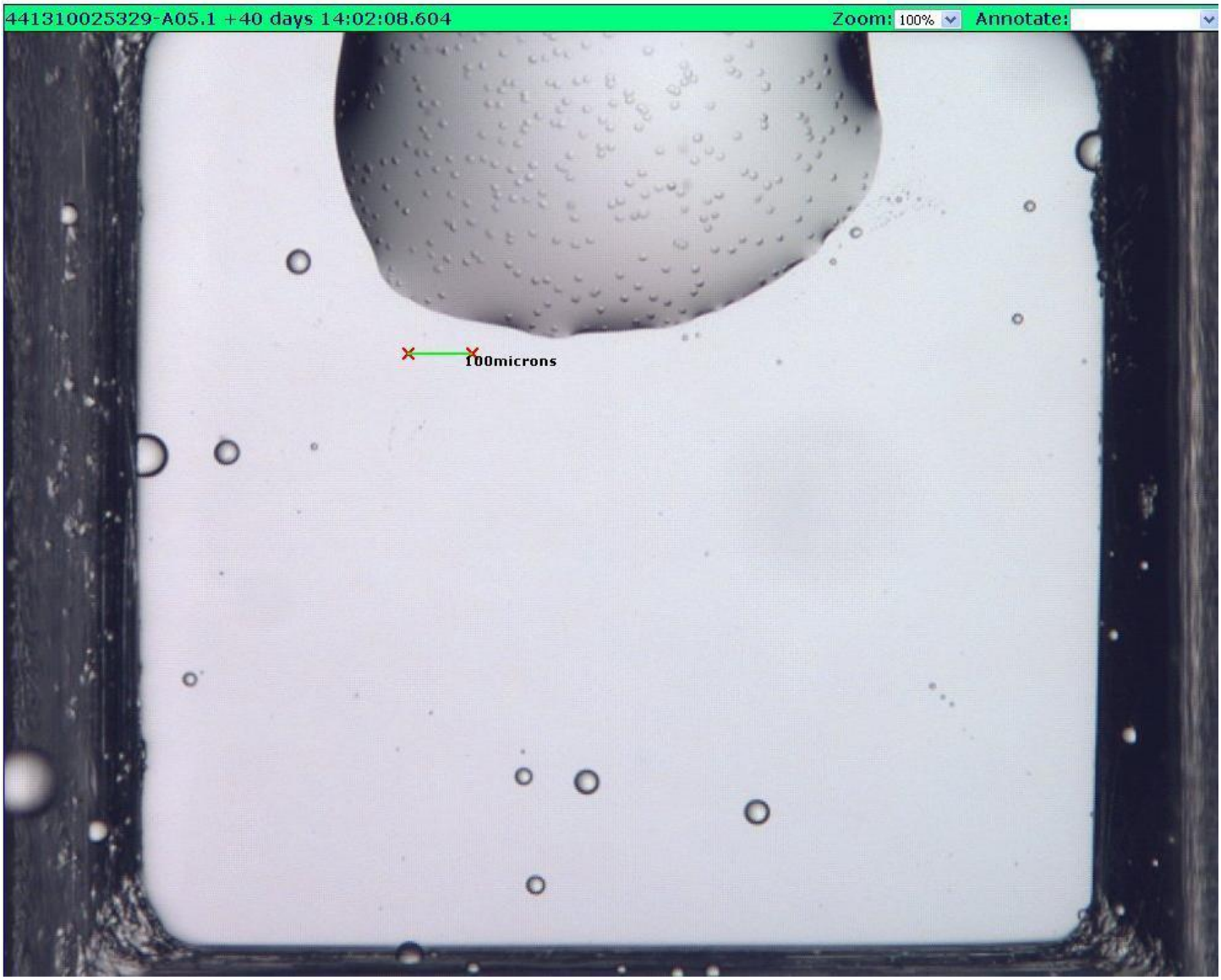


**Supplementary Figure 13**

BEV2 microcrystals.

Light microscope image of a small droplet containing BEV2 microcrystals. The size of the cubic crystals is approximately 8 x 8 x 8 $\mu m^3$.

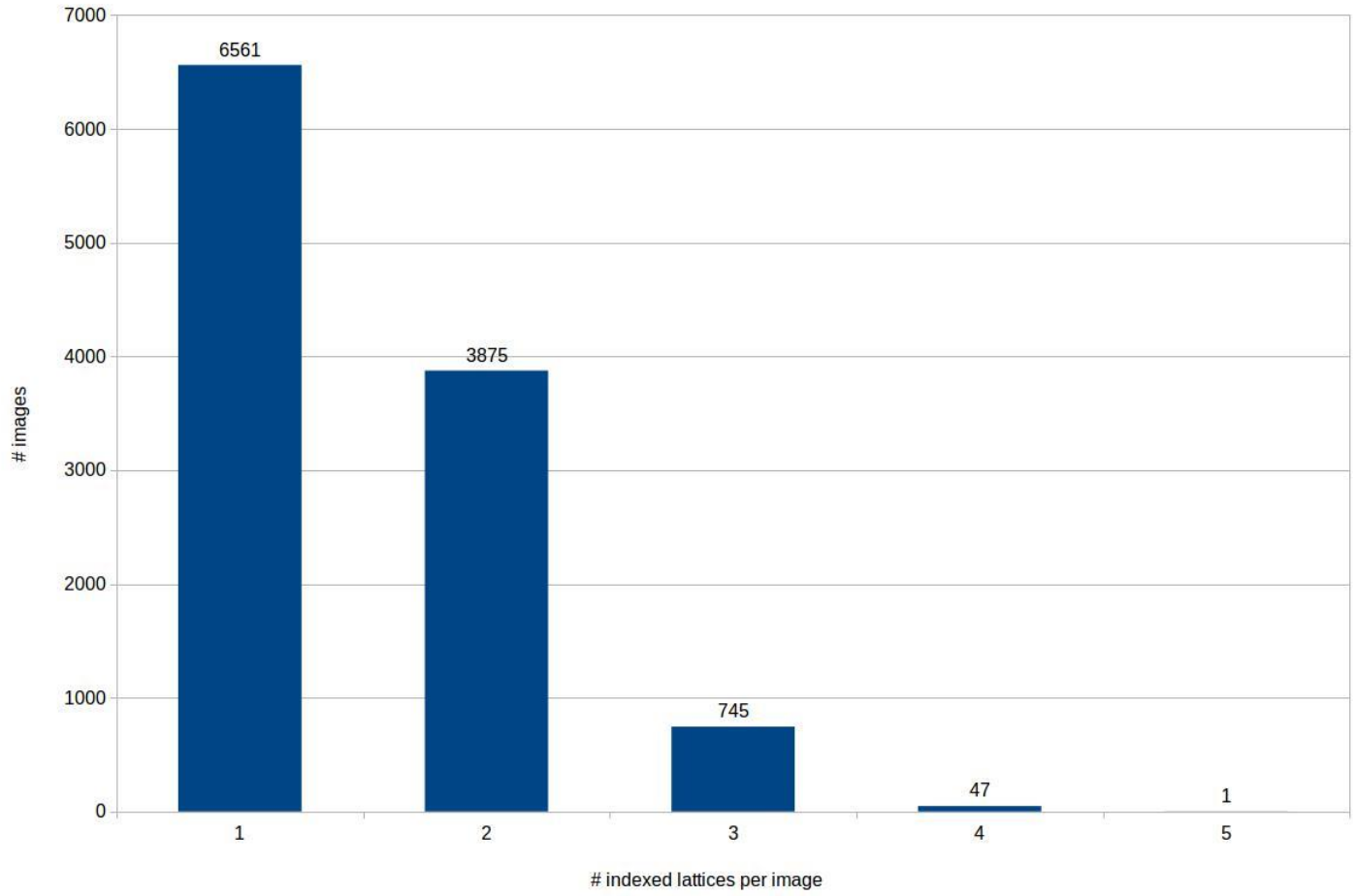


**Supplementary Figure 14**

Indexing results for CPV18 data.

Distribution of indexed lattices for CPV18 data (data collection run 47). From the 19028 recorded images, 13424 images were regarded as a hit (more than 20 strong spots). Due to multiple hits per shot, 16739 indexing solutions were found in total. As shown above, on 4668 images more than one indexing solution was present. For 6561 images, exactly one indexing solution was found.

**Supplementary Table 1:** Used parameters for DIALS spot finding. Full parameter definitions are available at the DIALS website (http://dials.lbl.gov/).

| **Parameter** | **BEV2** | **CPV18** |
|---|---|---|
| Gain | 14 | 14 |
| Global threshold | 2000 | 150 |
| Minimum spot size | 2 | 2 |
| Sigma background | 30 | 10 |
| Sigma strong | 6 | 8 |

**Supplementary Table 2:** Data collection and refinement statistics.

| | **BEV2** | **CPV18** |
|---|---|---|
| **Data Collection** | | |
| Temperature | 293 K | 100 K |
| Number of measured chips | 5 | 1 |
| Number of collected images | 8812 | 19028 |
| Total measuring time (s) | 818.6 | 566.1 |
| Average acquisition rate (images/s) | 10.79 | 33.61 |
| Number of hits | 446 | 13424 |
| Indexed patterns | 352 | 16739 |
| Number of lattices used in final merge | 324 | 9293 |
| Space group | F23 | I23 |
| Cell dimensions | | |
| a = b = c (Å) | 436.6 | 102.8 |
| α = β = γ (°) | 90 | 90 |
| Resolution (Å) | 29 – 2.3 (2.37 – 2.3)* | 30 – 2.4 (2.44 – 2.4)* |
| I/σ(I) | 5.4 (2.1) | 18.7 (6.2) |
| Completeness (%) | 82.1 (83.6) | 100 (100) |
| Redundancy | 2.3 (2.4) | 113.9 (24.9) |
| $R_{split}$ | 0.486 | 0.092 |
| $CC_{1/2}$ | 0.746 | 0.993 |
| **Refinement** | | |
| Resolution (Å) | 29 – 2.3 | 29.7 – 2.4 |
| No. reflections | 223989 (11604)** | 7231 (358)** |
| $R_{work}/R_{free}$ | 23.3/25.7 | 11.3/14.5 |
| No. atoms | 6587 | |
| Protein | 6212 | 1998 |
| Ligand/ion | 37 | 68 |
| Water | 338 | 172 |
| B-factors | | |
| Protein | 32 | 17.5 |
| Ligand/ion | 39 | 31.2 |
| Water | 38 | 22.8 |
| R.m.s. deviations | | |
| Bond lengths (Å) | 0.011 | 0.003 |
| Bond angles (°) | 1.6 | 0.75 |

*Values in parentheses are for highest-resolution shell.
** Values in parentheses are number of reflections used for $R_{free}$ calculation.